THE JOURNAL OF PHYSICAL CHEMISTRY B

Article

pubs.acs.org/JPCB

Charge-Transfer Mobility Parameters in Photoelectronic Devices: The Advanced Miller–Abrahams Computation

M. V. Basilevsky,*[,†] A. V. Odinokov,[†] and K. G. Komarova[†,‡]

[†]Photochemistry Center, Russian Academy of Sciences, ul. Novatorov 7a, Moscow 119421, Russia

[‡]Moscow Engineering Physics Institute, National Research Nuclear University, Kashirskoe sh. 31, Moscow 115409, Russia

ABSTRACT: The local hopping step of the electron transfer (ET) reaction is investigated for a real organic material composed of molecules M (*N*,*N*′-di(1-naphthyl)-*N*,*N*′-diphenyl-(1,1′-biphenyl)-4,4′-diamine). This material is implemented in light-emitting photoelectronic devices. The conductivity effect is simulated and calculated at a molecular level. We have studied the ET mechanism alternative to that suggested by the usually employed Marcus-like polaron model. The ion-molecular binary complex M^+M (for hole transfer) is considered as a reaction center. The reaction dynamics is carried through the low-frequency intermolecular vibration coordinate connecting its fragments (the promotion mode). Its coupling to the acoustic phonon bath serves for a dissipation of the reaction energy misfit. The high-frequency intramolecular vibrations (the reorganization modes) modulate the reaction kinetics via Franck–Condon factors induced by their polarization. The ET rate constants are evaluated in terms of the computational algorithm described earlier (Basilevsky, M. V.; et al. *J. Chem. Phys.* **2013** *139*, 234102). Standard quantum-chemical and molecular dynamical techniques are used for a calculation of all necessary parameters of this model. The macroscopic charge-carrier mobility of the material is estimated by properly averaging the rate constants over the total simulation cell.

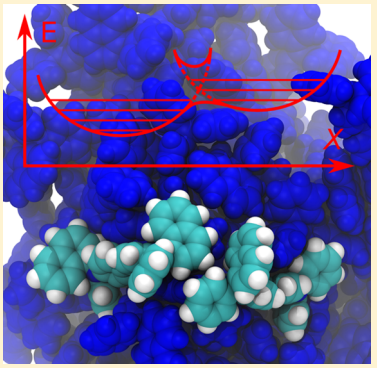

1. INTRODUCTION

Theoretical simulation of charge-carrier mobility in disordered solid matrices constituted of organic materials is an actively developing branch of recent research.[1−11] The practical importance of this problem stems from the fact that such systems provide a background for various photoelectronic devices transforming electricity into light (organic light-emitting diodes) and backward (photovoltaics). The electron-transfer (ET) reaction presents the key microscopic process that modulates and controls the charge mobility in such systems at a molecular level. In the subsequent text, the term "ET" is used with its extended meaning, including molecular transport of charges, both negative and positive.

The ET kinetics depends crucially on the mechanism involved in the interaction between the reaction partners and their surrounding environment. The mechanism in which the electron variables are directly coupled to medium polarization modes with continuum frequency spectrum (the polaron mechanism) is thoroughly elaborated.[12−18] The phenomenological description, valid as a high-temperature limit for the ET proceeding in polar liquids (Marcus, 1956) found its advanced development in terms of the radiationless transition theory (Levich and Dogonadze, 1959). This well-known MLD (Marcus–Levich–Dogonadze) theory is widely used in applications related to the theme of the present work.[3,7−11] We specially mention the more recent technical development of the Levich–Dogonadze approach in terms of the continuum integration methodology[19−21] (the so-called "spin-boson model").

An alternative ET model involved coupling of electron coordinates to acoustic phonon modes and was addressed for treating electron conductivity generated by impurities in crystalline lattice. Suggested by Miller and Abrahams[22] (the Miller–Abrahams (MA) theory) at a purely phenomenological level, it was applied to charge-transport problems in disordered organic semiconductors.[4,6,8,10] Its advanced microscopic formulation was not available for a long time. (In the present context, the term "advanced" means that the role of local molecular modes as a mediator between electron and phonon variables must be revealed and that the characteristics of the continuum frequency spectrum of the medium must be explicitly included in the consideration.) Such a model for the ET has been formulated recently,[23] although similar approaches for treating H-atom-transfer reactions were previously known.[24−30]

In the present work we report the ET rate constant computations based on the advanced MA methodology. A real practically important conducting material is considered. Its molecular-level background is represented by *N*,*N*′-di(1-naphthyl)-*N*,*N*′-diphenyl-(1,1′-biphenyl)-4,4′-diamine (*α*-NPD; see Figure 1). This organic semiconductor with high hole conductivity has been considered and investigated by both experimental and computational methods.[31,32] All incoming

Special Issue: John R. Miller and Marshall D. Newton Festschrift

Received: November 5, 2014
Revised: December 29, 2014

ACS Publications © XXXX American Chemical Society

DOI: 10.1021/jp5110714
J. Phys. Chem. B XXXX, XXX, XXX–XXX

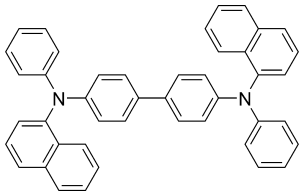

Figure 1. Chemical structure of α-NPD.

parameters including those that characterize the phonon frequency spectrum are computed explicitly by quantum-chemical (QC) and molecular dynamical (MD) methods.

A description of the model introduced in ref 23 is given in Section 2 for a consistency of the presentation. The main original contribution, including computations of parameters and rate coefficients, is contained in Sections 3 and 4. The concluding Section 5 summarizes the results and discusses possible applications.

2. HOPPING CONDUCTIVITY MODEL

a. General Description. The ET reaction center is immersed in a disordered molecular environment as shown in Figure 2. Uncharged molecules are randomly arranged around

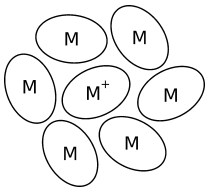

Figure 2. Charge-donor ion and its neutral environment.

cation M^+, and each dimeric pair is considered independently. Being quite sensitive to a particular dimer structure, a strongly fluctuating environment appears as a result. When a charge travels within an extended piece of material, such a situation reproduces itself step by step, creating a complicated bunch of 1D paths representing a multistep ET process.

The mobility of charge carriers is proportional to their effective diffusion constant to be revealed in a numerical procedure of averaging individual random trajectories.[6,8,9,11,33] The distribution of rate constants representing elementary local charge shifts serves as an input information for such a computation. The present work suggests a detailed prescription for treating this preliminary stage.

Let us consider in more detail the mechanism of the elementary step. It starts from the intramolecular reorganization of the dimeric fragments. This is aimed at preparing, for a given interfragment orientation, a dimer electronic structure that is as symmetric as possible. Electronic distributions within fragments conform to a particular geometrical dimer structure. Distortions within a charged and uncharged fragments are similar, but they proceed in different directions, which doubles the intrafragment reorganization energies. The interfragment ET appears as the next step. Its energetic effect Δ is measured relative to a previously symmetrized electronic structure and is expected to be small in magnitude. Medium reorganization makes a minor contribution to it.[11,23]

The total transition involves both electronic and local vibrational modes. We denote as x a collection of important electronic variables. Vibrational coordinates are denoted as X_k. For a collection $X = \{X_k\}$ the basis vibronic wave function consists of electronic and vibrational components: $\chi_1(x)\varphi_n(X)$ and $\chi_2(x)\varphi_{n'}(X)$. The electronic indices (1 and 2) and vibrational ones (n and n') label initial and final reaction states. The transition amplitude is considered within Franck–Condon (FC) approximation as

$$A_{nn'} = A_{12}\langle\varphi_n|\hat{A}_X|\varphi_{n'}\rangle \tag{1}$$

The electronic factor A_{12} is termed as "transfer integral".

The Fermi golden rule is a background for the rate computation[15−18]

$$K(T) = \frac{2\pi}{\hbar}\frac{C(T)}{Z(T)} \tag{2}$$

where $K(T)$ is the rate constant, $C(T)$ is the reactive transition flux, and $Z(T)$ is the normalization factor called "partition function" henceforth. Vibrational levels for X_k modes are broadened owing to the mode/medium interaction. This results in continuous energy distributions $\rho_n(E)$ and $\rho_{n'}(E)$. The flux and the partition function are expressed in terms of these distributions.[23,29]

b. Single-Mode ET Mechanism. As previously stated, the individual ET process in a particular ion-molecular dimer (Figure 2) involves two stages. The essence of the first (preparatory) stage is polarization of dimer fragments in opposite directions. The involved intrafragment vibrations are called "reorganization modes". The next stage, that is, the charge transfer between the fragments, is modulated by the interfragment vibration, called "promotion mode".

The operating mechanisms are different for reorganization and promotion modes. Correspondingly, coupling operators $\hat{A}_X$ in eq 1 are dissimilar. For a reorganization mode, the shift δ of its equilibrium position X_0 is the underlying factor ($\hat{A}_X = \exp(-\delta(\mathrm{d}/\mathrm{d}X))$). For the case of promotion mode another mechanism is postulated

$$\hat{A}_X = \exp[-\mu(X - X_0) - \nu(X - X_0)^2] \tag{3}$$

with adjustable parameters μ and ν. The equilibrium position remains unchanged and further we contract the notation as $(X - X_0) \rightarrow X$.

We consider next at a dynamical level only the single promotion mode X with frequency ω_0. The notation is changed as $X_k \rightarrow Y_k$ for the reorganization modes. It is supposed that frequencies ω_k of dynamically important reorganization modes are large, that is, $\omega_k \gg \omega_0$. Such situation is typical of real photoelectronic materials,[1−3,7−11] and this is confirmed by the forthcoming calculations (Section 4). We apply the FC principle once again to postulate that the kinetic impact of reorganization modes comes out only in terms of renormalization of the transition amplitude A_{12}. This can be performed by extending the standard Dogonadze–Jortner techniques[17,18,34,35] for the case of single active reorganization mode Y_r with frequency ω_r, coordinate shift δ_r, and wave functions $\varphi_n(Y_r)$. The exchange of n' energy quanta between modes X and Y_r results in the partial rate constant $K(T|\Delta + n'\hbar\omega_r)$, whereas the total rate result reads

$$K(T) = \sum_{n'=0} \langle\phi_0(Y_r)|\phi_{n'}(Y_r + \delta_r)\rangle^2 \cdot K(T|\Delta + n'\hbar\omega_r) \tag{4}$$

where the first term is the standard FC factor. The partial rates are calculated as the usual promotion rate constant (eq 2) with

DOI: 10.1021/jp5110714
J. Phys. Chem. B XXXX, XXX, XXX−XXX

a correspondingly changed energy misfit Δ. All other specific parameters, namely, ω_0, μ, ν, g, and b, remain unchanged.

c. Relaxation as the Origin of Level Broadening. Symbolically, the ET reaction is represented as

$$(x, X, Y)_{1n} \rightarrow (x, X, Y)_{2n'} + \Delta \tag{5}$$

The subscripts label initial and final reaction states. The energetic misfit Δ is released or absorbed due to the dimer/medium interaction. This is illustrated by Figure 3. The two

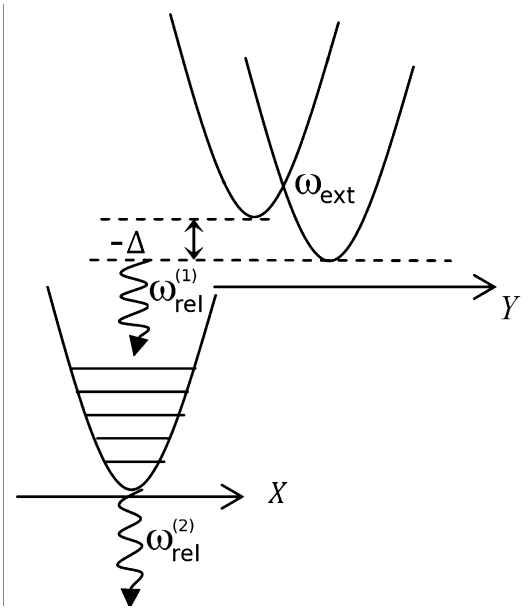

Figure 3. Scheme of reaction 5. High-frequency coordinate Y tunnels with frequency ω_{ext}. Its energy misfit Δ is transferred from Y to X (frequency $\omega_{ext}^{(1)}$) and next from X to the medium.

upper potential wells represent a purely electronic transition performed by means of the fast reorganization modes Y_k. They are separated by the potential barrier, and the related electron tunneling is characterized by the transition frequency ω_{ext}. The top of the barrier corresponds to the transition-state geometry distorted owing to the shifts of soft reorganization modes. The charge-transferring tunneling of fast modes proceeds at this point, after which the distorted transition geometry slides down into the product well. Intrawell vibronic interactions are separated as FC factors in eq 4. No more impact of fast reorganization modes on the reaction kinetics is allowed. The stationary regime with constant reaction flux establishes the magnitude of the total rate $K(T)$ owing to the interplay between the under-barrier tunneling and the relaxation of the resonance misfit Δ. There exist two relaxation frequencies that control the energy exchange. The first one ($\omega_{rel}^{(1)}$) is responsible for the energy exchange between modes X and Y (eq 4 simulating this step in terms of a single effective mode Y_r). The relaxation frequency $\omega_{rel}^{(2)}$ is determined by the bilinear interaction of the local mode X and acoustic medium phonon modes Q_ν

$$W(X, Q_\nu) = XQ; \quad Q = \sum_\nu c_\nu Q_\nu \tag{6}$$

The collective medium mode Q has a dimension of force constant and appears as a random force perturbing the dynamics of the promotion mode X. Medium modes represent the continuous spectrum of frequencies ω_ν. Thereby, the relaxation frequency ω_{rel} is controlled by the distribution of amplitudes $c_\nu = c(\omega_\nu)$, that is, the so-called spectral density.[20] The following computational algorithm invokes the spectral function $\rho_n(t)$

$$\rho_n(t) = \frac{1}{2\pi} \exp\left[-\frac{\Gamma_n}{2} f(t)\right]$$

$$\Gamma_n = (2n + 1) \coth \frac{\hbar\omega_0}{2k_B T} - 1$$

$$f(t) = g\left[|t| + \frac{1}{b}(e^{-b|t|} - 1)\right] \tag{7}$$

This form is extracted for each vibrational level n as a solution of the relaxation equation in the Redfield approximation.[23,36] The distributions $\rho_n(E)$, which determine the reaction flux and the partition function in eq 2, can be derived as Fourier transforms of $\rho_n(t)$ in eq 7. The widths Γ_n are different for levels with n = 0, 1, ..., whereas the universal function $f(t)$ is n-independent; its form is borrowed from the theory of vibrational band shapes[37] and called "the Kubo function" in the forthcoming text. Parameters g and b represent the intensity of interaction and the shape of the spectral band.

3. COMPUTATIONAL METHODOLOGIES

a. Vibrational FC Factor. The FC overlap integrals in eq 4 are expressed[38] in terms of Huang–Rhys parameters $S_k = (\lambda_k/\hbar\omega_k)$, where $\lambda_k = (1/2)m_k\omega_k^2\delta_k^2$ is the reorganization energy for mode Y_k with mass m_k, frequency ω_k, and coordinate shift δ_k. So

$$\langle\phi_0(Y_k)|\phi_n(Y_k + \delta_k)\rangle = \left(e^{-S_k}\frac{(S_k)^n}{n!}\right)^{1/2} \tag{8}$$

The computation followed ref 39. The normal modes for a neutral NPD molecule were found at its ground-state potential energy minimum point disregarding the medium environment. The pertaining cation geometry was calculated in terms of the restricted Kohn–Sham method for open-shell systems. We used DFT quantum-chemical computations with PBE0 functional[40] and the Gaussian-type basis 6-311G(d,p)[41] implemented in Firefly QC package,[42] which is partially based on the GAMESS(US)[43] source code.

b. Electron Coupling Parameters and Their Distance Dependence. The computation of electronic amplitude A_{12} (eq 1) used the tight-binding model as described in ref 44. This approach constructs the electron wave function of a charged dimer M^+M based on MOs of its neutral monomer fragments. The charge appears in terms of orbital populations. The HF/6-31G* computational level was implemented in terms of GAMESS US.[43] The SCF procedure was performed first for each monomer function inside the dimer. The vectors of MO coefficients, extracted from output files, were then used to construct the basis set of dimer MOs having doubled dimension. The missing coefficients were substituted by zeroes. The Fock matrix and the overlap matrix were computed with this basis set without performing a preliminary SCF procedure. The transfer integral A_{12} was then evaluated in terms of off-diagonal elements of the Fock matrix. This procedure includes the symmetric orthogonalization of the monomer orbitals.[8,44]

This method was successfully applied for ET computations in various chemical objects. However, when materials specific for organic electronics are considered, some methodological

DOI: 10.1021/jp5110714
J. Phys. Chem. B XXXX, XXX, XXX–XXX

Table 1. Computation of Rate Constants and Its Input Parameters

no.	A_{12} (10^{-2} eV)	μ (nm^{-1})	ω_0 (cm^{-1})	b/ω_0	g/ω_0	$<X^2>$ (nm^2)	$\Delta^{(HOMO)}$ (eV)[a]	$\Delta^{(el)}$ (eV)[b]	$K(T)$ (s^{-1}), eq 2	$K(T)$ (s^{-1}), eq 5[c]
1	0.85	20.1	155	47.8	2.24	0.021	−0.53	−0.31	5.49×10^{12}	8.96×10^{8}
2	1.51	17.0	218	12.2	1.72	0.020	−0.22	−0.47	2.80×10^{13}	1.30×10^{10}
3	1.09	16.0	183	17.6	2.08	0.023	−0.08	−0.04	$2,79 \times 10^{12}$	6.50×10^{6}
4	2.68	28.1	190	37.6	1.50	0.019	−0.40	−0.68	7.80×10^{16}	3.37×10^{13}
5	2.29	3.4	187	12.0	2.02	0.019	−0.76	−0.69	3.17×10^{9}	1.27×10^{9}
6	2.55	13.6	236	11.2	1.60	0.019	−0.24	−0.01	1.93×10^{13}	3.81×10^{7}
7	0.93	23.2	149	22.3	2.30	0.034	−0.18	−0.14	8.42×10^{10}	3.51×10^{9}
8	1.94	34.6	158	20.8	1.84	0.022	−1.24	−0.04	3.09×10^{16}	9.47×10^{10}

[a]HOMO approach (see Section 3c). [b]Electrostatic field effect (eq 9). [c]Hyang−Rhys parameter for mode Y_r in eq 4 is doubled; see the text.

problems may appear. Typically, such materials consist of large organic molecules having similar intramolecular subfragments (i.e., those inside a monomer molecule, see the structure of α-NPD (Figure 1), for example). Such a situation often generates a subset of quasi-degenerate orbitals, built of combinations of subfragment HOMOs and LUMOs. Depending on the environment, the variation of relative positions and orientations of those subfragments in a real amorphous material produces varying subsets of monomer MOs, which are quasi-degenerate, and all are active in the ET. There exists four such active monomer MOs in the case of α-NPD. The energy splitting within this subset is on order of k_BT, whereas the energy gap separating them from the remainder array of inactive MOs is on order of 1 eV. Thereby, we obtain 4 ways of different localization of active MOs within a monomeric unit and 16 possibilities of their combination in a dimer. Actually, many charge localization patterns are involved within the present single-electron model in the ET process under consideration.

We resolved this problem by invoking the magnitude of transfer integral A_{12} as a proper localization criterion. Its large value indicates that the charge is localized at the pair of monomer subfragments, which contact closely in a given dimer. Among 16 differently localized MO pairs the one that has the biggest value of A_{12} is mainly responsible for the ET. This prescription looks reliably under the condition that intramolecular ET proceeds much more rapidly than the intermolecular one.

The distance dependence of the ET amplitude (eq 3) was evaluated as follows. We considered the distance between centers of mass of dimer fragments (the other coordinates being fixed) as an effective promotion mode. The distance X between the mass centers was shifted twice along the pertaining vector by 0.02 Å in both directions. The A_{12} value was computed at each dimer configuration. The resulting dependence, approximated in terms of eq 3, provided its parameter μ (the parameter ν being disregarded). This μ value was calibrated by the optimization including five distance steps.

c. Distribution of Resonance Misfits. The misfit Δ is the difference between energies of final and initial electronic states of a charged dimer complex appearing in the hole transfer process $M^+M \rightarrow MM^+ + \Delta$. Its average vanishes in a symmetric system, the fluctuations arising owing to random changes of conformations for a monomer fragment M as promoted by its environment. The pertaining energy change is described conventionally as a variation of the vertical ionization potential of M, that is, as a random variation of its HOMO energy[45] depending on a position of a hopping site. Such sort of computation is very approximate and yields extremely large values of the Δ variance. (See Table 1.) Within a more accurate approach, taking into account the total change of the electronic structure promoted by ionization, extremely small variance (10^{-2} eV) was obtained for Alq3.[11] Thereby, we considered as doubtful the results of computations by means of the first method and neglected them at the background of a much larger effect produced by the second source of fluctuations. This is the nonuniform electric field modulated by the random local environment. It adds the electrostatic energy correction for misfit Δ located at site i where the monomer M is located

$$\Delta_i^{(el)} = \sum_{ai} \sum_{j} \sum_{bj} \frac{(q_{ai}^c - q_{ai}^n) q_{bj}}{\varepsilon_\infty |r_{ai} - r_{bj}|} \tag{9}$$

Indices ai and bj label the atoms of two M's belonging to sites i and j, respectively. Atomic charges q_{ai}^c and q_{ai}^n correspond to the charged and neutral forms of molecule M. The use of optical dielectric permittivity ε_∞ accounts for the dielectric screening owing to the electronic polarization of monomer molecules. This screening procedure was proved to be legitimate provided the atomic site coordinates in eq 9 are extracted from a nonpolarizable MD trajectory.[46,47] The value of ε_∞ =3 is typical for organic semiconductors.[11]

d. Details of Molecular Dynamics Computations. Parameters of atom−atom interactions for α-NPD were borrowed from the GAFF force field.[48] The atom typization and preparation of files including molecular topologies and force-field parameters was performed automatically by means of procedures involved in program package Amber Tools.[49] Atomic partial charges were calculated with RESP[50] methodology based on the HF/6-31G* computation. The cubic simulation cell contained 50 α-NPD molecules. After preliminary heating up to 500 K and the following annealing to 0 K the cell edge length 3.58 nm was obtained. The ultimate model of amorphous α-NPD arrived after geometry optimization in the frame of conjugated gradient method. In simulations the integration step was 1 fs and all covalent bonds including hydrogen atoms were constrained (the LINCS algorithm[51]). The system was relaxed in a velocity rescaling thermostat[52] (0.3 ps time constant) and in a Berendsen barostat (0.5 ps time constant) under the equilibrium pressure of 1 bar. The cutoff 1.2 nm constant was used for the truncation of intermolecular interactions. Long-distance electrostatic interactions were treated in terms of the PME method.[53] The dispersion correction was added to the system energy and to its virial. The program package GROMACS 4.6[54] was used.

e. Extraction of Relaxation Parameters. For the promotion mode X with spectral function (eq 7) we simulated its velocity ($u(t) = \dot{X}$) autocorrelation function, normalized to unity at the time origin (i.e., $C(t) = \langle u_0 u_t \rangle / \langle u_0^2 \rangle$), as[37]

DOI: 10.1021/jp5110714
J. Phys. Chem. B XXXX, XXX, XXX−XXX

$$C(t) = \exp\left\{-\frac{g}{2}\left[|t| + \frac{1}{b}(e^{-b|t|} - 1)\right]\right\} \exp(i\omega_0 t) \quad (10)$$

Parameters g, b, and ω_0 were fitted in a MD simulation. The special computation of 200 ps length with T = 298 K and constant pressure 1 bar was performed. The coordinates and velocities of all atoms were recorded every 5 fs. The distance between centers of mass of the dimer fragments was considered to be X. The velocity vector was extracted at each step by means of MDAnalysis library.[55] For fitting the correlation function we used the initial piece of the MD trajectory starting from t = 0 and up to the first minimum of $C(t)$. The further trajectory analysis is difficult due to strong fluctuations. The so found value of ω_0 characterizes the effective (screened by the medium) frequency of X mode.

4. RESULTS AND DISCUSSION

a. Transfer Integrals. The MD simulation for the amorphous α-NPD material was arranged as described in Section 3c. The cell containing 50 molecules is shown in Figure 4. The transfer integral A_{12} was then calculated for each of 1225

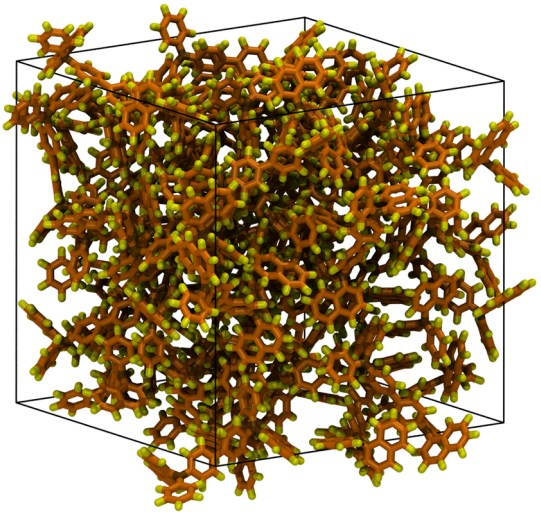

Figure 4. MD model of amorphous α-NPD material.

dimer configurations contained in the cell. Altogether 402 nonzero values have been observed. The distribution for this array is shown in Figure 5. The main peak (A_{12} > 6.6 × 10^{-4} eV) is clearly distinguished; it covers about one-half of all dimer

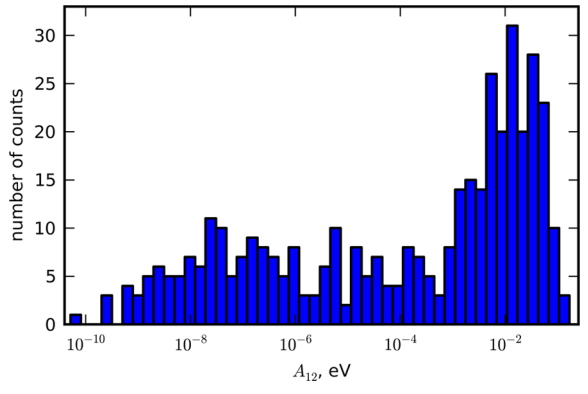

Figure 5. Distribution of transfer integrals A_{12}.

samples. On average, each α-NPD molecule has seven neighbors keeping the transfer integral within the main peak. This suffices to postulate the percolation transfer mechanism that allows one to consider as negligibly small the contributions to the charge mobility coming from the distribution tails.

b. FC Factors. The computed values of Huang–Rhys parameters $S_k = (\lambda_k/\hbar\omega_k)$ (see eq 10) are shown in Figure 6.

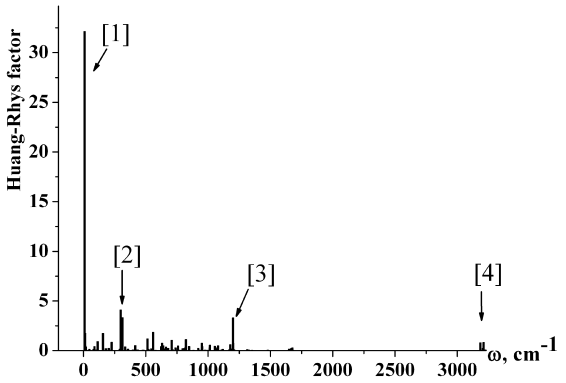

Figure 6. Huang–Rhys factors of normal modes for neutral-cation geometry shift versus their frequencies. [1] ω_i = 9 cm^{-1} torsional vibration of amino-groups; [2] ω_i =298 and 313 cm^{-1} out-of-plane skeletal vibrations of N–Ph–Ph–N phenylene-groups; [3] ω_i = 1200 cm^{-1} C–H scissoring vibrations; and [4] ω_i = 3184 and 3211 cm^{-1} C–H stretching vibrations.

They reflect the geometry rearrangement due to shift δ_k promoted by the transformations of two α-NPD molecules, entering as partners in the M^+M complex, when one of them changes from the neutral to charged state and the other one changes oppositely. The intramolecular reorganization modes Y_k with frequencies ω_k were subdivided into fast ones ($\omega_k > \omega_T$) and soft ones ($\omega_k < \omega_T$), where the thermal frequency $\omega_T = (k_BT/\hbar) \approx 200$ cm^{-1}. Only high-energy modes are counted in terms of eq 4 ($S_k > 1$ and $\omega_k \geq 300$ cm^{-1}).

The unpaired electron is located on phenyl rings of the bridge –N–Ph–Ph–N– (Figure 1), and the most essential geometry distortions were observed within this region of α-NPD molecule. So the bond length between the phenyl rings changes from 1.48 to 1.45 Å, and the two C–N bonds change between 1.42 and 1.38 Å when M transforms into M^+. As a result, the Huang–Rhys parameters for fast modes are ω_k = 298 cm^{-1}, S_k = 4.27 and ω_k = 313 cm^{-1}, S_k = 3.40 (wagging vibrations of phenyls); ω_k = 558 cm^{-1}, S_k = 2.02 (wagging vibrations of nitrogen atoms); ω_k = 1200 cm^{-1}, S_k = 3.35 (C–H scissoring vibrations); ω_k = 3.184 cm^{-1}, S_k = 0.77 and ω_k = 3.211 cm^{-1}, S_k = 2.02 (stretching C–H vibrations). The contributions of all these modes to the ET kinetics are collected in eq 4. The main impact of soft modes ($\omega_k < \omega_T$) is to modify the molecular geometry, and the soft mode (ω_k = 9 cm^{-1}), representing the torsional vibrations of amino groups, makes the largest contribution to the geometry distortion (S_k = 32).

c. Rate Computations. To give an illustration, we randomly selected eight dimer pairs for a computation of the ET rate constant $K(T)$ (Section 2). They were sampled from the main peak of the distribution shown in Figure 5. The interaction between promotion and reorganization modes was treated in terms of eq 4. The high-temperature Redfield approximation[23] was applied for the partial rates.

Table 1 contains the rate values so found together with parameters required for such a calculation. Quantities A_{12}, μ,

DOI: 10.1021/jp5110714
J. Phys. Chem. B XXXX, XXX, XXX–XXX

ω_0, b, g, and Δ are described in Section 2. Also shown is the mean-squared fluctuation for the mode X position. It determines the magnitude of the important quantity $c = (\mu L_0)^2$, where $l_0 = (\hbar/m\omega_0)^{1/2}$ is the zero-level vibrational amplitude. This dimensionless parameter is a measure of the intensity of interlevel transitions introduced by the coupling operator (no. 3). Numerically, $c = \mu^2\langle X^2\rangle(\hbar\omega_0/k_BT)$ is obtained from a MD simulation.

Additional discussion is required regarding the energy misfit Δ. It has the vanishing average for the present symmetric ET process (Section 3c). Its fluctuations generated by the environment appear as random conformational changes that are clearly observable in the MD trajectory underlying Figure 4. In a crude approximation, this effect can be interpreted as a fluctuation of the instantaneous ionization potential of dissolved M fragments, that is, as a change of their HOMO energy. On the basis of the computations for Alq3[11,43] we concluded in Section 3c that so computed Δ values are strongly exaggerated on average. This has found a support in our present computations for a-NPD (Table 1) with the variance equal to 0.43 eV. Therefore, only the electrostatic effect (eq 9) was counted in Δ values designed for final rate computations. A resulting Δ variance of 0.20 eV was found for the distribution so obtained. Computations of Δ performed by the two methods are compared in Table 1.

Some more information on the same theme can be extracted from the experimental data. For typical organic semiconductors the Δ magnitude does not exceed 0.1 to 0.15 eV.[56] The results reported in Table 1 are slightly higher, which could be explained by the spurious increase in dipole moments arising as a flaw of the HF/6-31G* calculations required by the consistent application of the GAFF force field.

A comment about rate computations addresses a different point. The dynamical impact of reorganization modes was introduced via eq 4. We consider the total frequency range in terms of the qualitative concept of "fast" and "soft" modes with the boundary $\omega = \omega_T = k_BT/\hbar$ between them.[17,20,57] Two intensive fast modes (frequencies $\omega_1 = 1200$ cm^{-1} and $\omega_2 = 300$ cm^{-1}) can be detected in Figure 6. They show the largest Huang–Rhys amplitudes. However, only a single fast mode (namely, ω_1) can be included under the technique of [4]. Its two-mode extension[11] requires a significantly larger computational effort which was unavailable in the context of the present work based on the advanced algorithm for multiple rate calculations (as compared with simple Marcus-like rate expressions as used in ref 11). An argument in defense of such a simplification can be deduced from the general rule[17,56] that only fast modes are involved in nonadiabatic transitions, whereas the mission of soft modes is to modify the potential energy relief. The first mode (ω_1), implemented as a fast one in eq 4, corresponds to CH bond vibrations with small amplitude and thus weakly interferes with environment motions.[58] The second mode (ω_2) has the same Huang–Rhys intensity, but it belongs to large amplitude wagging vibrations of phenyl rings (see Section 4c), which are active for varying, by means of the interference with medium motions, the random conformations of α-NDP molecules. According to such criterion, this mode, located close to the formal soft/fast boundary, is transferred to the family of soft modes, which are responsible for conformational fluctuations of the Δ misfit, as previously discussed. An important comment about the active reorganization mode Y_r states that its Huang–Rhys parameter must be doubled[11] (S_r = 6.70, see Section 4b) because this mode appears twice in the dimer vibrational wave function.

d. Mobility Estimation. If the percolation regime is assumed for the charge diffusion, then the mobility can be estimated in terms of the diffusion constant D as[7,8]

$$\text{mobility} = eD/k_BT \tag{11}$$

where e means the charge of its carrier. Under the assumption on the drift of a single charge with no external field, one obtains, after combining the contributions from all dimer pairs (i,j)[59]

$$D = \frac{1}{2nN}\sum_{i,j} r_{ij}^2 \frac{K_{ij}^2}{\sum_{j'} K_{ij'}} \tag{12}$$

Here r_{ij} and K_{ij} denote separation distances (along X) and the hopping rate constants for a given pair (i, j), $n = 3$ is the space dimension, and $N = 50$ is the number of α-NPD particles in the MD cell.

For the total array of ET pairs, our rate computations were reduced to a simplified and unified scheme. Parameters A_{12} and Δ were introduced individually for each particular pair. Specification of other parameters is not so important, and it was made based on the inspection of data in Table 1. So, averaged parameters $\langle X^2\rangle$, g, and ω_0 were taken for all rates. The average was also accepted for parameter μ, after withdrawing point 5 of Table 1, which seems to be out of range. The spectral shape parameter b is more specific, and the rates were computed with its two limiting values, $b = 10$ and 50, to reveal its importance for the final rate result.

In Table 2, the mobility results obtained from the present rate calculations are compared with those using standard

Table 2. Charge Carrier Mobilities

computational methodology		mobility ($cm^2\ V^{-1}\ s^{-1}$)	
		K_{ij} from eq 2	K_{ij} from eq 4
Marcus formula	λ_{out} = 0.05 kcal/mol	2.5	4.34×10^{-3}
	λ_{out} = 0.2 kcal/mol	2.9	2.69×10^{-3}
advanced Miller–Abrahams approach	b = 10	267	1.62×10^{-2}
	b = 50	160	1.22×10^{-2}
experiment	ref 61	3.2×10^{-3}	
	ref 62	2.9×10^{-4}	
	ref 63	6.1×10^{-4}	

Marcus rate computation. The latter ones, except transfer integrals A_{12} and Δ (as computed in the present work), need the values of outer-sphere reorganization energies λ_{out}. Their evaluation requires either extended quantum-chemical treatment or the knowledge about a polarizable force field for a given material. Both sources were unavailable for the present case. The tentative estimates in Table 2 are based on the data for λ_{out} obtained for similar materials (polycyclic aromatic molecules providing λ_{out} in the range 0.05 to 0.2 kcal/mol[60]).

The comparison between Marcus and the advanced MA schemes was motivated by a simple physical argument inquiring whether polaron or acoustic phonon mechanism is more adequate for judging the mobility laws in disordered organic materials.[23] The present attempt is not complete for several reasons.

(1) The key parameters (especially the energy misfits) are not quite definite.

DOI: 10.1021/jp5110714
J. Phys. Chem. B XXXX, XXX, XXX–XXX

(2) It is observed[23] that the Marcus rates are always overrated, as compared with the similar (i.e., with the same parametrization) advanced MLD approach. The distinction increases rapidly with the temperature decrease. The full MLD treatment is desirable for making an unbiased comparison between the two ET mechanisms.

(3) Most uncertain in rate computations is the stage of adding, in terms of FC factors, the kinetic impact of fast reorganization modes (eq 4). The effect proved to be extremely large (Table 1). The extension of this procedure for several modes (even for two modes[11]) requires too much computational effort. The further rate reduction is expected but its significance remains vague.

(4) A possible deficiency of the present simple treatment of charge mobility (eq 12) might become visible as compared with sophisticated kinetic Monte Carlo procedures used for this purpose in several other studies.[7−9,11,33]

(5) The experimental mobility data are known within an order of magnitude (Table 2).

A comparison between the MA and Marcus approaches is not straightforward owing to different physical models they suggest for the energy exchange between the ET reaction center and the medium. They introduce quite different parameters in the corresponding stages of the rate computation. Such is outer-sphere reorganization energy λ_{out} (Marcus) versus parameters μ, g,and b in the MA scheme. Parameters μ and g depend slightly on the environment. (See Table 1, where we eliminate from the discussion the seemingly spurious line 5.) The parameters λ_{out} and b (controlling the spectral line shape as introduced in the MA approach) are quite sensitive to the neighbor variation around the ET dimer pair. However, it is seen from Table 2 that such variations make relatively little impact on averaged ET rates. The systematic mobility trends remain stable within both approaches.

From a computational point of view the treatment of the system/medium interaction is simpler in the MA algorithm. The Marcus computation of λ_{out} requires polarizable force fields, whereas the velocity autocorrelation function, underlying the computation of the shape parameter b, is available by the MD simulation with fixed atomic charges.

The last comment returns to the specific role of soft intramolecular modes. They are generally expected to modify the classical potential energy relief, providing an effective barrier for tunnel transitions of fast modes.[17] Assuming that the energy misfit is negligible in average, this results in a symmetric Marcus barrier created by the soft modes (Figure 3), that is, $U_r = \lambda_r/2$, where λ_r represents the sum of reorganization energies over the modes with frequencies $\omega_r < 200$ cm^{-1} (the thermal frequency), counted for the pair of fragment partners for the reacting dimer. The probability factor $P = \exp(-U_r/k_BT)$ measures the transition-state population for activated dimers. It amounts to $\sim 10^{-1}$ with $\lambda_r = 0.1$ eV, as extracted from computations of Section 3c. (Note that the total λ_r, including fast modes as well, is estimated to be 0.3 eV.) This effect renormalizes the MA rates and mobilities listed in Tables 1 and 2. The frequency variation modulated by the dimer environment is neglected in the present tentative estimate (which is also disregarded when considering the fluctuation of energy misfits which issued from the same origin). The expected correction would increase the frequencies and further reduce the P factor.

Provided the alternative MLD mechanism is considered, the Marcus λ_r contributed by the soft modes (i.e., 0.1 eV) should be added to the reorganization energy associated with the polarization mode. This would change the Marcus barrier height and the rates. The significance of such correction can be estimated from Table 2.

5. CONCLUSIONS

The MA mechanism is frequently used as an easy route for a simulation of ET rates in disordered solid matrices composed of organic materials.[4−8,33] It serves as an alternative to the Marcus-like methodologies, which, as previously pointed out,[23] have unclear physical background in such systems. From the point of the rate theory, in all solid-phase applications the both approaches appear in their simplified phenomenological versions.

The present study suggests a microscopic framework for the MA method by formulating it as an advanced rate computation in terms of the promotion mode. The practice of this work shows that an advanced computation is indeed realizable and desirable even for complicated applications. This opens the perspective for studying by a simulation the dependences of the charge mobility on the temperature and the applied electric field. A similar extension is, of course, also available for the Marcus-like mechanisms, by applying it in the full advanced MLD formulation for local reorganization modes, which can now be performed within the same rate algorithm.[23] The only modification required for such tests is the different calibration of the phonon spectrum parameters, which, in the case of the polaron ET mechanism, must be extracted from the frequency-dependent and complex-valued dielectric permittivity[17,18,64,65] rather than from a simulation of the velocity correlation function, as in the present work. We also note that our rate algorithm, being valid under ordinary temperature conditions, is not fully adapted for the low-temperature kinetic regime.[23] Further elaboration of these techniques is required as a matter for the future work. The unified consideration of both MLD and MA reaction mechanisms also seems not impossible by the combination of the algorithm[23] with that developed in ref 28 for H-transfer reactions.

AUTHOR INFORMATION

Corresponding Author

*E-mail: basil@photonics.ru.

Notes

The authors declare no competing financial interest.

ACKNOWLEDGMENTS

We thank Prof. A. A. Bagaturyants and Prof. M. V. Alfimov for stimulating discussions on the problem of ET transfer in solid state. This work was supported by the Russian Science Foundation, contract no. 14-43-00052.

REFERENCES

(1) *Organic Electronics*; Klauk, H., Ed.; Wiley-VCH: Berlin, 2006.

(2) *Organic Photovoltaics*; Brabec, C., Scherf, U., Dyakonov, V., Eds:, Wiley-VCH: Berlin, 2008.

(3) *Organic Semiconductors in Sensor Applications*; Bernards, D. A., Owens, R. M., Malliaras, G. G., Eds:, Springer: Berlin, 2008.

(4) Bässler, H. Charge Transport in Disordered Organic Photoconductors. A Monte Carlo Simulation Study. *Phys. Status Solidi B* **1993**, *175*, 15−56.

(5) Fishchuk, I. I.; Kadashchuk, A.; Bässler, H.; Nespurek, S. Nondispersive Polaron Transport in Disordered Organic Solids. *Phys. Rev. B* **2003**, *67*, 224303.

DOI: 10.1021/jp5110714
J. Phys. Chem. B XXXX, XXX, XXX−XXX

(6) Bässler, H.; Emelianova, E. V. Steady State Photoconduction in Amorphous Organic Solids. *Adv. Polym. Sci.* **2010**, *223*, 1−28.
(7) Brédas, J.-L.; Beljonne, D.; Coropceanu, V.; Cornil, J. Charge -Transfer and Energy Transfer Processes in π-Conjugated Oligomers and Polymers. A Molecular Picture. *Chem. Rev.* **2004**, *104*, 4971−5003.
(8) Coropceanu, V.; Cornil, J.; da Silva Filho, D. A.; Oliver, Y.; Silbey, R.; Bredas, J.-L. Charge Transfer in Organic Semiconductors. *Chem. Rev.* **2007**, *107*, 926−952.
(9) Nelson, J.; Kwiatkowski, J. J.; Kirkpatrick, J.; Frost, J. M. Modeling Charge Transport in Disordered Organic Materials. *Acc. Chem. Res.* **2009**, *42*, 1768−1778.
(10) Baranovskii, S. D.; Rubel, O.; Jansson, F.; Österbaka, R. Description of Charge Transport in Disordered Organic Materials. *Adv. Polym. Sci.* **2010**, *223*, 45−71.
(11) Rühle, V.; Lukyanov, A.; May, F.; Schrader, M.; Verhoff, T.; Kirkpatrik, J.; Baumeier, B.; Andrienko, D. Microscopic Simulation of Charge Transport in Disordered Organic Semiconductors. *J. Chem. Theory Comput.* **2011**, *7*, 3335−3345.
(12) Marcus, R. A.; Sutin, N. Electron transfers in chemistry and biology. *Biochim. Biophys. Acta* **1985**, *811*, 265−322.
(13) Marcus, R. A. On the Theory of Oxidation-Reduction Reactions Involving Electron Transfer. I. *J. Chem. Phys.* **1956**, *24*, 966−978.
(14) Marcus, R. A. On the Theory of Electron-Transfer Reactions. VI. Unified Treatment for Homogeneous and Electrode Reactions. *J. Chem. Phys.* **1965**, *43*, 679−701.
(15) Levich, V. G.; Dogonadze, R. R. Theory of Nonradiation Electron Transitions from Ion to Ion in Solutions. *Dokl. Akad. Nauk SSSR* **1959**, *124*, 123−126.
(16) Levich, V. G.; Dogonadze, R. R. Adiabatic Theory of the Electron Transfer Processes in Solutions. *Collect. Czech. Chem. Commun.* **1961**, *26*, 193−214.
(17) Ulstrup, J. *Charge Transfer in Condensed Media*; Springer: Berlin, 1979.
(18) Bixon, M.; Jortner, J. Electron Transfer − from Isolated Molecules to Biomolecules. *Adv. Chem. Phys.* **1999**, *106*, 35−202.
(19) Leggett, A. J.; Chakravarty, S.; Dorsey, A. T.; Fisher, M. P. A.; Garg, A. Dynamics of Dissipative Two-State Systems. *Rev. Mod. Phys.* **1987**, *59*, 1−85.
(20) Weiss, U. *Quantum Dissipative System*, 2nd ed.; World Scientific: Singapore, 1999.
(21) Lang, G.; Palladino, E.; Weiss, U. Electron Transfer in Non-Adiabatic Regime: Crossover from Quantum-Mechanical to Classical Behavior. *Chem. Phys.* **1999**, *244*, 111−125.
(22) Miller, A.; Abrahams, E. Impurity Conduction at Low Concentrations. *Phys. Rev.* **1960**, *120*, 745−755.
(23) Basilevsky, M. V.; Odinokov, A. V.; Titov, S. V.; Mitina, E. A. Golden Rule Kinetics of Transfer Reactions in Condensed Phase. The Microscopic Model of Electron Transfer Reactions in Disordered Solid Matrices. *J. Chem. Phys.* **2013**, *139*, 234102.
(24) Trakhtenberg, L. I.; Klochikhin, V. I.; Pshezhetski, S.Ya. Theory of Tunnel Transitions of Atoms in Solids. *Chem. Phys.* **1982**, *69*, 191−198.
(25) Goldanski, V. I., Trakhtenberg, L. I., Flerov, V. N. *Tunneling Phenomena in Chemical Physics*; Gordon and Breach: New York, 1989.
(26) Trakhtenberg, L. I.; Fokeyev, A. A. Pressure and Temperature Dependence of H-Atom Tunneling in the Debye Approximation. Barrier Preparation and Media Reorganization. *J. Phys. Chem. A* **2007**, *111*, 9509−9515.
(27) Suarez, A.; Silbey, R. Hydrogen Tunneling in Condensed Media. *J. Chem. Phys.* **1991**, *94*, 4809−4816.
(28) Ohta, Y.; Soudakov, A. V.; Hammes-Shiffer, S. Extended Spin-Boson Model for Non-adiabatic Tunneling in the Condensed Phase. *J. Chem. Phys.* **2006**, *125*, 144522.
(29) Basilevsky, M. V.; Davidovich, G. V.; Voronin, A. I. Non-Markovian Modification of the Golden Rule Rate Expression. *J. Chem. Phys.* **2006**, *125*, 194513.
(30) Basilevsky, M. V.; Tikhomirov, V. A. Computation of the Tunneling H-Transfer Reaction Kinetics in the Fluorene Molecular Crystal. *Mol. Phys.* **2008**, *106*, 2391−2405.
(31) Chauhan, G.; Srivastava, R.; Kumar Rai, V.; Kumar, A.; Bawa, S. S.; Srivastava, P. C.; Kamalasanan, M. N. Thermally activated field assisted carrier generation and transport in N,N′-di-[(1-naphthalenyl)-N,N′-diphenyl]-(1,1′ biphenyl)-4,4′-diamine doped with 2,3,5,6-tetrafluoro-7,7′,8,8′-tetracyanoquinodimethane. *J. Appl. Phys.* **2008**, *104*, 124509.
(32) Wang, Z. B.; Helander, M. G.; Greiner, M. T.; Qiu, J.; Lu, Z. H. Carrier mobility of organic semiconductors based on current-voltage characteristics. *J. Appl. Phys.* **2010**, *107*, 034506.
(33) Korolev, N. A.; Nikitenko, V. R.; Ivanov, D. V. Quasi-equilibrium hopping drift and field-stimulated diffusion in ultrathin layers of organic materials. *Physics and Techniques of Semiconductors* **2010**, *45*, 230−235.
(34) Dogonadze, R. R.; Itskovich, E. M.; Kuznetsov, A. M.; Vorotyntsev, M. A. Theory of light absorption by ions in solution. *J. Phys. Chem.* **1975**, *79*, 2827−2834.
(35) Kestner, N. R.; Logan, J.; Jortner, J. Thermal Electron Transfer Reactions in Polar Solvents. *J. Phys. Chem.* **1974**, *78*, 2148−2165.
(36) Pollard, W.; Felts, A. K.; Friesner, R. A. The Redfield Equation in Condensed Phase Quantum Dynamics. *Adv. Chem. Phys.* **1996**, *93*, 77−134.
(37) Kubo, R.; Toda, M.; Hashitsume, N. *Statistical Physics II. Nonequilibrium Statistical Mechanics*; Springer Verlag: Berlin, 1985.
(38) Medvedev, E. S.; Osherov, V. I. *Radiationless Transitions in Polyatomic Molecules*; Springer-Verlag: Berlin, 1995.
(39) Vragovich, J.; Calzado, E. M.; Diaz Garcia, M. A. The structure and energetics of TPD ground and excited states. *Chem. Phys.* **2007**, *332*, 48−54.
(40) Adamo, C.; Barone, V. Toward reliable density functional methods without adjustable parameters: The PBE0 model. *J. Chem. Phys.* **1999**, *110*, 6158−6170.
(41) Krishnan, R.; Binkley, J. S.; Seeger, R.; Pople, J. A. Self-consistent molecular orbital methods. XX. A basis set for correlated wave functions. *J. Chem. Phys.* **1980**, *72*, 650−654.
(42) Granovsky, A. A. *Firefly*, version 8. http://classic.chem.msu.su/gran/firefly/index.html.
(43) Schmidt, M. V.; Baldridge, K. K.; Boatz, J. A.; Elbert, S. T.; Gordon, M. S.; Jensen, J. H.; Koseki, S.; Matsunaga, N.; Nguyen, K. A.; Su, S.; et al. General atomic and molecular electronic structure system. *J. Comput. Chem.* **1993**, *14*, 1347−1363.
(44) Valeev, E. F.; Coropceanu, V.; da Silva Filho, D. A.; Salman, S.; Bredas, J.-L. Effect of Electronic Polarization on Charge-Transfer Parameters in Molecular Organic Semiconductors. *J. Am. Chem. Soc.* **2006**, *128*, 9882−9886.
(45) Lee, C.; Waterland, R.; Sohlberg, K. Prediction of Charge Mobility in Amorphous Organic Materials through the Application of Hopping Theory. *J. Chem. Theory Comput.* **2011**, *7*, 2556−2567.
(46) Leontyev, I. V.; Vener, M. V.; Rostov, I. V.; Basilevsky, M. V.; Newton, M. D. Continuum Level Treatment of Electronic Polarization in the Framework of Molecular Simulations of Solvation Effects. *J. Chem. Phys.* **2003**, *119*, 8024−8037.
(47) Leontyev, I. V.; Stuchebrukhov, A. A. Electronic Continuum Model for Molecular Dynamics Simulations. *J. Chem. Phys.* **2009**, *130*, 085102.
(48) Wang, J.; Wolf, R. M.; Caldwell, J. W.; Kollman, P. A.; Case, D. A. Development and testing of a general amber force field. *J. Comput. Chem.* **2004**, *25*, 1157−1174.
(49) Case, D. A.; Babin, V.; Berryman, J. T.; Betz, R. M.; Cai, Q.; Cerutti, D. S.; Cheatham, T. E., III; Darden, T. A.; Duke, R. E.; Gohlke, H., et al.*AMBER 14*; University of California: San Francisco, CA, 2014.
(50) Bayly, C. I.; Cieplak, P.; Cornell, W. D.; Kollman, P. A. A well-behaved electrostatic potential based method using charge restraints for deriving atomic charges: the RESP model. *J. Phys. Chem.* **1993**, *97*, 10269−10280.
(51) Hess, B.; Bekker, H.; Berendsen, H. J. C.; Fraaije, J. G. E. M. LINCS: A linear constraint solver for molecular simulations. *J. Comput. Chem.* **1997**, *18*, 1463−1472.

DOI: 10.1021/jp5110714
J. Phys. Chem. B XXXX, XXX, XXX−XXX

(52) Bussi, G.; Donadio, D.; Parrinello, M. Canonical sampling through velocity rescaling. *J. Chem. Phys.* **2007**, *126*, 014101.
(53) Essmann, U.; Perera, L.; Berkowitz, M. L.; Darden, T.; Lee, H.; Pedersen, L. G. A smooth particle mesh Ewald method. *J. Chem. Phys.* **1995**, *103*, 8577−8593.
(54) Abraham, M. J.; van der Spoel, D.; Lindahl, E.; Hess, B.; GROMACS development team. *GROMACS User Manual*, version 5.0.2, 2014. www.gromacs.org.
(55) Michaud-Agrawal, N.; Denning, E. J.; Woolf, T. B.; Beckstein, O. MDAnalysis: A toolkit for the analysis of molecular dynamics simulations. *J. Comput. Chem.* **2011**, *32*, 2319−2327.
(56) Nikitenko, V. R.; Strikhanov, M. N. Transport level in disordered organics: An analytic model and Monte-Carlo simulations. *J. Appl. Phys.* **2014**, *115*, 073704.
(57) Kuznetsov, A. M. Role of High-Frequency and Low-Frequency Polarization of the Medium in the Kinetics of Electron Transfer and Thermodynamics of Solvation. *J. Phys. Chem.* **1992**, *96*, 3337−3345.
(58) Li, H.; Duan, L.; Zhang, D.; Qiu, Y. Influence of Molecular Packing on Intramolecular Reorganization Energy: A Case Study of Small Molecules. *J. Phys. Chem. C* **2014**, *118*, 14848−14852.
(59) Deng, W.-Q.; Goddard, W. A. Predictions of Hole Mobilities in Oligoacene Organic Semiconductors from Quantum Mechanical Calculations. *J. Phys. Chem. B* **2004**, *108*, 8614−8621.
(60) McMahon, D. P.; Troisi, A. Evaluation of the External Reorganization Energy of Polymers. *J. Phys. Chem. Lett.* **2010**, *1*, 941−946.
(61) Ruhstaller, B.; Carter, S. A.; Barth, S.; Riel, H.; Riess, W.; Scott, J. C. Transient and steady-state behavior of space charges in multilayer organic light-emitting diodes. *J. Appl. Phys.* **2001**, *89*, 4575−4586.
(62) Nguyen, N. D.; Schmeits, M. Determination of charge-carrier transport in organic devices by admittance spectroscopy: Application to hole mobility in α-NPD. *Phys. Rev. B* **2007**, *75*, 075307.
(63) Brütting, W.; Riel, H.; Beierlein, T.; Riess, W. Influence of trapped and interfacial charges in organic multilayer light-emitting devices. *J. Appl. Phys.* **2001**, *89*, 1704−1712.
(64) Ovchinnikov, A. A.; Ovchinnikova, M. Ya. Contribution to the Theory of Elementary Electron Transfer Reactions in Polar Liquids. *Sov. Phys. JETP* **1969**, *29*, 688−693.
(65) Basilevsky, M. V.; Chudinov, G. E. Oscillator Hamiltonian Representation of the Linear Response Theory for Stochastic Outer-Sphere Electron Transfer Reactions. *J. Chem. Phys.* **1995**, *103*, 1470−1480.

DOI: 10.1021/jp5110714
J. Phys. Chem. B XXXX, XXX, XXX−XXX